



Biofloat observations of a phytoplankton bloom and carbon export in the Drake Passage



Alexander R. Davies^{a,*}, Fabrice Veron^b, Matthew J. Oliver^b

^a Oceanography Department, U.S. Naval Academy, Annapolis, MD 21402, USA

^b School of Marine Science and Policy, University of Delaware, Lewes, DE 19958, USA

ARTICLE INFO

Keywords:

Biological pump
Southern Ocean
Carbon export
Biofloat
Mesoscale eddies

ABSTRACT

Prolonged in-situ biogeochemical observations have historically been limited in the high nitrate, low chlorophyll (HNLC) regions of the Southern Ocean (SO). Recently, large biofloat missions, including the SO Carbon and Climate Observations and Modelling (SOCCOM) program, are filling the data void. However, the standard ten-day float profiling cycle often lacks the temporal resolution required to resolve mesoscale phytoplankton bloom or export processes. This is particularly important in regions of the SO dominated by high energy mesoscale features, like the Drake Passage. In this study, we observe a naturally occurring phytoplankton bloom and subsequent carbon export event in the Drake Passage using in-situ data from an Autonomous Profiling EXplorer (APEX) biofloat that profiled the water column every two days. The fast, two-day profiling cycle meant that the biofloat's trajectory was coherent with mesoscale processes. However, because of the quasi-Lagrangian nature of the biofloat, we could not control for both spatial and temporal changes simultaneously. Therefore we explore this quasi-Lagrangian dataset as both a spatial and temporal series to understand the mesoscale processes as they relate to the observed phytoplankton bloom and its subsequent export. Our evidence suggests that eddy-driven subduction and a change in the vertical structure were important in the time period leading up to enhanced carbon export. Recent studies have shown that eddy-driven subduction may be responsible for ~20% of the total biological carbon pump in the SO. We estimate that the POC flux out of the surface ocean was $250 \pm 50 \text{ mg m}^{-2} \text{ d}^{-1}$ between the peak bloom through an observed export event. In addition, we estimate that $\sim 18 \pm 10\%$ of the particulate organic carbon observed during the peak bloom was exported out of the surface ocean via subduction and sinking.

1. Introduction

Carbon dioxide (CO₂) exchange across the air-sea interface occurs on relatively short timescales, with turnover times for atmospheric CO₂ in the surface ocean on the order of one to ten years. Air-sea CO₂ fluxes are primarily controlled by wind forcing and CO₂ disequilibrium, which is in-part controlled by biochemical surface ocean variability. In the open ocean, the pycnocline acts to inhibit vertical exchanges between the surface and deep ocean, including the long term, deep ocean sequestration of atmospheric CO₂. One mechanism for transporting carbon from the surface to deep ocean is the biological pump. In well-lit regions of the surface ocean (the euphotic zone), phytoplankton convert CO₂ into particulate organic carbon (POC) that can form aggregates and sink below the pycnocline into the deep ocean. In the deep ocean, the POC is either respired back to dissolved CO₂ or the organic carbon reaches the ocean floor and is buried in the sediment.

The natural phytoplankton abundance in the open waters of the Southern Ocean (SO) is seasonally light limited (El-Sayed, 1987) and, in austral summer, characterized by intense, patchy phytoplankton blooms (Moore and Abbott, 2000; Arrigo et al., 2008). Natural (Blain et al., 2007; Pollard et al., 2009) and artificial (Boyd et al., 2000; Gervais et al., 2002; Coale et al., 2004; Hiscock and Millero, 2005; Hoffmann et al., 2006; Harvey et al., 2010; Law et al., 2011; Smetacek et al., 2012; Martin et al., 2013) iron fertilization experiments have confirmed that the phytoplankton abundance across the SO is limited by insufficient surface iron concentrations (Martin, 1990; Martin et al., 1990). Furthermore, iron fertilization experiments have shown evidence for enhanced post-bloom carbon export (e.g. Blain et al., 2007; Smetacek et al., 2012).

Until recently, prolonged in-situ biogeochemical observations in high nitrate, low chlorophyll (HNLC) regions of the SO were sparse. The Argo float program (Argo Science Team, 1998) substantially enhanced

* Corresponding author.

E-mail address: adavies@usna.edu (A.R. Davies).

<https://doi.org/10.1016/j.dsr.2019.02.004>

Received 8 September 2017; Received in revised form 17 February 2019; Accepted 22 February 2019

Available online 26 February 2019

0967-0637/ Published by Elsevier Ltd.

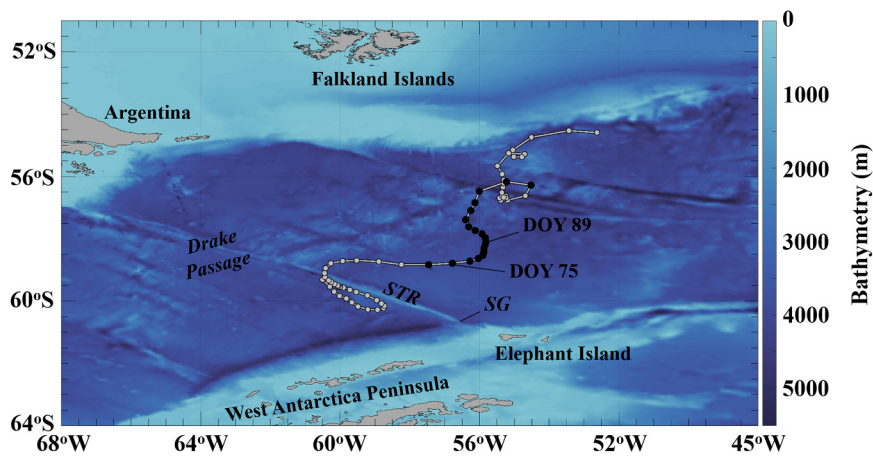


Fig. 1. Biofloat locations and trajectory over the entire deployment period (grey). Biofloat locations during the observational period (DOY 73–109) are plotted in black. Bathymetry is from the Global, Self-consistent, Hierarchical High-resolution Geography (GSHHG) database (Wessel and Smith, 1996). The Shackleton Transverse Ridge (STR) and Shackleton Gap (SG) are labelled. The Ona Basin is just east of the STR.

oceanic observational capabilities and data collection at the turn of the century via the continued deployment of thousands of autonomous floats that profile temperature and salinity every ten days. While the Argo program increased our understanding of the SO (Riser et al., 2016), observations remained relatively limited compared with other ocean basins due to seasonal ice cover. In addition, the floats initially lacked biogeochemical sensors. New initiatives, including the SO Carbon and Climate Observations and Modelling (SOCCOM) program, aim to fill the data void with hundreds of biogeochemical float (herein biofloat) deployments in the open SO and within the seasonal ice zone. Biofloats have increased our understanding of SO biogeochemical processes (Hennon et al., 2016; Briggs et al., 2017; Johnson et al., 2017; Williams et al., 2017; Llort et al., 2018), instrument techniques and biases (Haëntjens et al., 2017; Johnson et al., 2017b), seasonal and annual variability (Kamenkovich et al., 2017; Williams et al., 2018) and climate processes (Jones et al., 2016; Mazloff et al., 2017).

A limited, but scientifically fruitful, number of biofloat studies with high profiling frequencies (approximately 2 days) have focused on mesoscale biogeochemical processes in the SO. Bishop et al. (2004) was one of the first biofloat studies in the Australian sector of the SO and successfully observed the development of a mesoscale phytoplankton bloom and carbon export event following artificial iron injection. A follow-on study analyzed year-round biomass and carbon flux observations from four biogeochemical floats profiling the ocean daily (Bishop and Wood, 2009) whereby light availability, changes in the mixed layer depth, and zooplankton grazing were hypothesized to describe the onset of natural phytoplankton blooms in the Australian sector of the SO. Rembauville et al. (2017) deployed five high frequency profiling floats in the Indian Ocean sector of the SO in conjunction with shipboard sampling to understand mesoscale changes in plankton community composition from biofloat observations. The insights provided by these high frequency biofloat studies show the importance of mesoscale dynamics in understanding the processes driving phytoplankton bloom formation, export, and community composition in other parts of the SO.

One of the major findings resulting from autonomous system deployments is the relative importance of subduction in the biological pump. Gradient estimates of particulate nitrogen and nitrate from SOCCOM biofloats suggest that the total export from subduction is ~19% (Stukel and Ducklow, 2017). This is similar to estimates of POC flux in Llort et al. (2018), who identified eddy-driven subduction events from biofloats using apparent oxygen utilization and temperature-salinity (TS) properties. These eddy-driven export processes were clustered around regions of high eddy kinetic energy, like the Kerguelen Plateau. However, because the floats were sampling on 3–10 day cycles, it was difficult to resolve the mesoscale processes associated with the export events. While the sampling rate of a given float is not impacted by the kinetic energy or currents in the ambient environment, the drifting

nature of floats often means that areas of high eddy kinetic energy, like the Drake Passage, may be under sampled. This highlights the need for strategic deployments in these regions (Llort et al., 2018).

In this study, we deployed a high frequency profiling biofloat in the Drake Passage and observed a naturally occurring phytoplankton bloom and subsequent carbon export event. The Drake Passage is characterized by high mesoscale kinetic energy, and is considered an HNLC region. Section 2 outlines methodology and data from an Autonomous Profiling EXplorer (APEX) biofloat that sampled the water column every two days. Throughout this study, we apply a quasi-Lagrangian analysis approach with respect to the biofloat dataset whereby both spatial and temporal changes cannot be simultaneously controlled (Section 2.3). In Section 3, we present results and discussion related to the naturally occurring phytoplankton bloom (3.1) and export (3.2) observed by the biofloat. In Section 4 we offer a summary and concluding remarks.

2. Data and methods

2.1. APEX biofloat

An APEX biofloat (Supplemental Fig. 1) was deployed in the Drake Passage on December 18, 2012 at 64.813°W and 59.870°S. In-situ data were collected from the beginning of January through in the beginning of June in 2013 (the deployment period) as the biofloat profiled the water column from 2000 dbar to the surface every two days. While most profiling floats sample on a ten-day cycle, the higher frequency profiling rate employed in this study allowed the biofloat to better resolve mesoscale processes. Between profiles, the biofloat was positioned at a park depth of 1000 dbar. During the profiling cycle, the biofloat was at the surface for on the order of one hour and at the park depth for on the order of one day. Fig. 1 shows the float trajectory and surface locations during the deployment period.

The biofloat measured vertical profiles of pressure, temperature, and salinity with a SeaBird model 41 CTD, along with optical backscatter, colored dissolved organic matter (CDOM) fluorescence (not shown), and chlorophyll-a fluorescence with a WET Labs Combination Fluorometer-Scattering-CDOM Sensor model ECO FLbbCD-74 AP2. Measurements above 500 dbar were made at approximately 5 dbar intervals for higher resolution sampling of the upper ocean. Pressure was converted to depth by assuming hydrostatic balance with one standard atmosphere of pressure at the ocean surface. The profile on day of year (DOY) 71 was eliminated from the analysis because it exhibited unrealistic and noisy density inversions. This was likely caused by a temporary blockage in the conductivity cell.

A three bin vertical running mean was applied to all variables to reduce noise (Llort et al., 2018). With a vertical bin resolution of approximately five meters in the upper ocean, this resulted in a fifteen

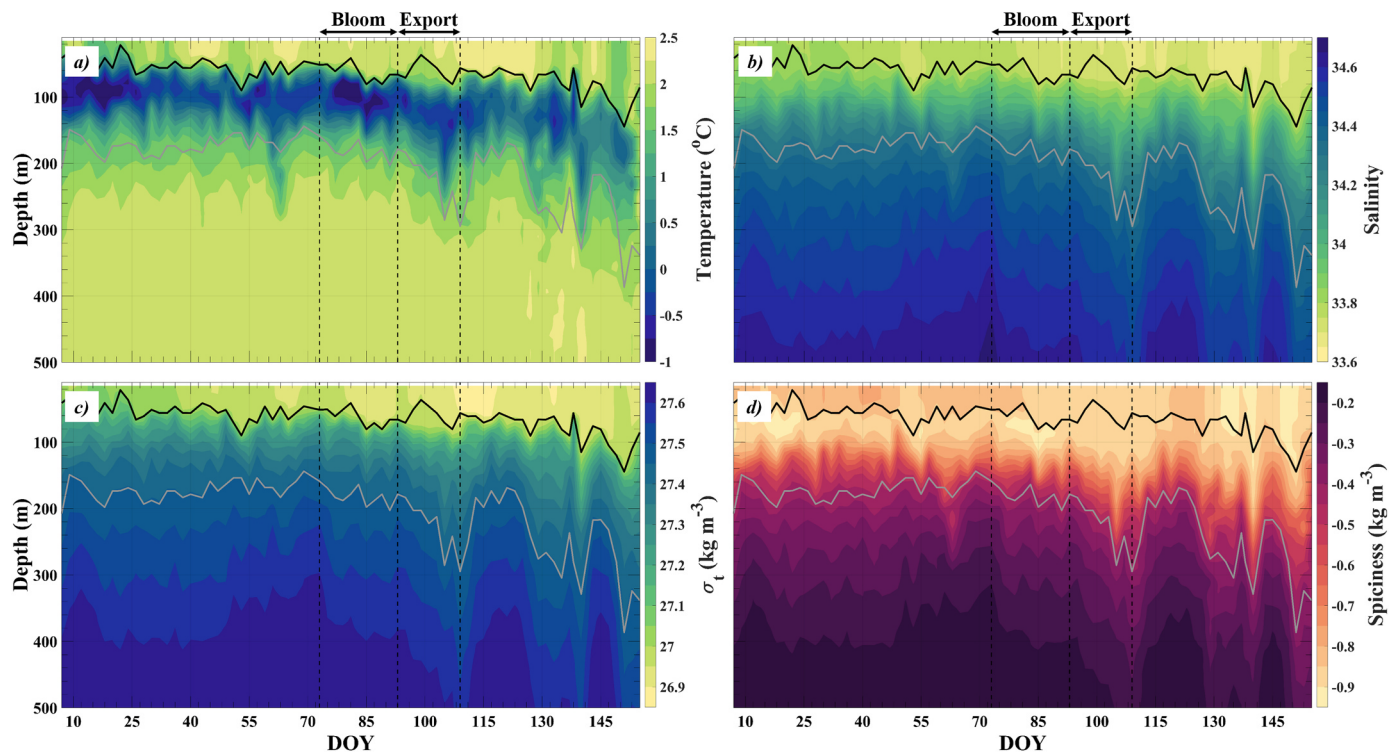


Fig. 2. Biofloat *a*) temperature, *b*) salinity, *c*) σ_t and *d*) spiciness observations from 500 m to the surface during the deployment period. In this figure, data profiles are linearly interpolated onto a vertical fixed grid with 5 m spacing. The mixed layer depth (black line), hereby defined as the depth at which the change in σ_t from the surface first exceeds 0.03 kg m^{-3} (Dong et al., 2008), and depth of the reference isopycnal (grey line defined as $\sigma_t = 27.45 \text{ kg m}^{-3}$), z_p , are plotted. The observations coincident with the timing of the observed phytoplankton bloom and export are labelled (see Fig. 3).

meter smoothing of the data. Recent studies have applied varying low pass filters to bio-optical profiles consisting seven bin vertical running means (e.g. Llort et al., 2018) or five bin running medians followed by seven bin running means (e.g. Briggs et al., 2011; Rembauville et al., 2017). Here we allow for higher frequencies in the bio-optical profiles to preserve some of the “spikiness” for comparison with Bishop and Wood (2009), while still achieving some smoothing appropriate for plankton flux estimates and analysis.

Fig. 2 shows the biofloat temperature, salinity, σ_t , and spiciness observations in the upper 500 m of the water column. $\sigma_t = \rho - 1,000$ where the density (ρ) is derived from temperature and salinity measurements following Gill (1982). Spiciness (Flament, 2002) is derived from potential temperature and potential density, and allows for comparing and differentiating between water mass with similar densities but potentially different thermohaline properties (Llort et al., 2018).

Fig. 3 shows the biofloat chlorophyll-*a* concentration ($[Chl]$), a proxy for phytoplankton abundance) and particulate organic carbon concentration ($[POC]$) observations in the upper 500 m of the water column. The biofloat surfaced at night to reduce the effects of non-photochemical quenching (NPQ) on fluorescence measurements. The community-established global calibration bias between chlorophyll-*a* concentration estimates from WET Labs ECO-series fluorometers and high performance liquid chromatography (HPLC) chlorophyll measurements is two (Roesler et al., 2017). However for the SO, Johnson et al. (2017b) found a bias of $6.4 (\pm \text{the larger of } 0.2 \text{ mg m}^{-3} \text{ or } 48\%)$. In this study, the raw chlorophyll-*a* concentration was calculated from the sensor fluorescence signal (per manufacture provided calibration corrections) and divided by 6.4 per Johnson et al. (2017b).

The backscattering coefficient of particles (b_{bp}) was calculated following techniques described in Johnson et al. (2017b) and references therein, and is often used as an optical proxy for particulate organic carbon concentration (e.g. Bishop and Wood, 2008; Boss et al., 2015). We employed a linear empirical relationship,

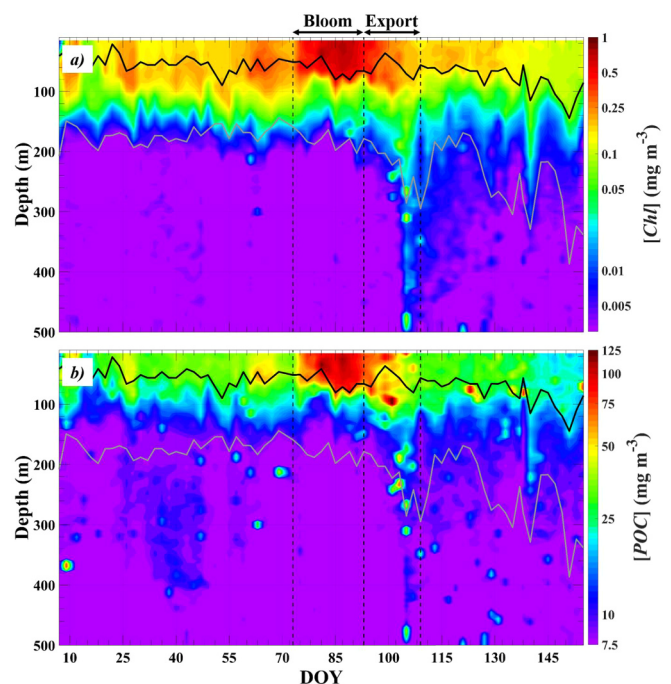


Fig. 3. Same as Fig. 2 but for *a*) chlorophyll concentration, $[Chl]$, and *b*) particulate organic carbon concentration, $[POC]$.

$[POC] = 3.12 \times 10^4 (\pm 2.47 \times 10^3) \times b_{bp} + 3.0 (\pm 6.8)$, to estimate the particulate organic carbon concentration (mg m^{-3}) from particle backscattering. This relationship was derived by Johnson et al. (2017b) in the upper 100 m of the surface ocean with an average error the larger of 35 mg m^{-3} or 20%.

For our analysis, we define the mixed layer depth (MLD) as the depth at which the change in σ_t from the surface first exceeds 0.03 kg m^{-3} (Dong et al., 2008). While we use this definition throughout this manuscript, reducing the complexity of density profiles to a single scalar number may not be a good proxy for all relevant upper ocean processes. Therefore, we choose an additional “reference isopycnal” for the upper ocean at $\sigma_t = 27.45 \text{ kg m}^{-3}$. The depth of this isopycnal (z_p) is located near the bottom of the pycnocline and is correlated with the depth of surrounding isopycnals (Fig. 2c). Thus, z_p is suitable for profile-to-profile comparisons of the pycnocline depth and the overall vertical structure of the upper ocean. While z_p was not selected for biological reasons, an additional benefit is that z_p approximates the deepest extent of the surface phytoplankton layer in each profile, with the obvious exception during the observed direct export event (Fig. 3) which is the topic of this manuscript and discussed in Section 3.2. This makes z_p a reasonable lower physical limit for depth integrating [Chl] and [POC] in the upper ocean.

2.2. OSCAR surface currents

The unfiltered, $1/3^\circ$ resolution, five-day averaged Ocean Surface Current Analysis–Real time (OSCAR currents; ESR, 2009) data product was used to better understand surface currents and physical processes within the Drake Passage. The OSCAR currents were estimated by combining a quasi-steady geostrophic model (derived from altimetry) with wind-driven ageostrophic currents and thermal wind adjustments. The currents are depth averaged to 30 m (see Bonjean and Lagerloef, 2002 for full model description) and are packaged as discrete, temporal blocks of five-day averaged currents. In this study we linearly interpolated the u (zonal) and v (meridional) OSCAR current components in time for a daily OSCAR current product. We further bi-linearly interpolated the daily $1/3^\circ$ resolution OSCAR currents on a sphere to the biofloat locations.

2.3. Quasi-Lagrangian analysis approach

Circulation across the much of the open SO is equivalent barotropic (Killworth and Hughes, 2002; Gille et al., 2007) which implies that while the strength of the observed surface currents may decrease with depth, the orientation likely does not (Llort et al., 2018). Indeed, even globally, the surface and park depth velocities from Argo floats profiling on the standard five- to ten- day schedules show a similar distributions (Ollitrault and Rannou, 2013). Therefore floats are considered “quasi-Lagrangian” with respect to mesoscale ocean circulation (Llort et al., 2018). In this study, we opted for a faster, two-day profiling cycle which theoretically allowed the biofloat to more readily resolve mesoscale processes that occur on the order of ten days in the SO (Daniault and Menard, 1985).

In Fig. 4 we compare the biofloat surface locations to the likely surface tracer trajectories (grey) derived from the OSCAR currents, along with an estimate of kinetic energy per unit mass (KE),

$$KE = \frac{1}{2}(u^2 + v^2). \quad (1)$$

Based on the one-third degree spatial resolution and five-day sampling period, OSCAR currents are well-suited to resolve the mesoscale dynamics in the SO which occur on the order of 100 km spatially and 10 days temporally (Daniault and Menard, 1985). The quasi-Lagrangian biofloat approximates the likely surface ocean trajectories (Fig. 4). Empirically, the largest discrepancies (both in distance and direction) during observational period (DOY 73–109) occurred in lower KE regimes, which was also coincident with the timing of the observed bloom. For additional context, we evaluated the ratio of the distance between the biofloat and coincident likely surface tracer locations (D_{if}) to the distance travelled by the likely surface ocean tracer between profiles (D_i). The ratio of D_{if} to D_i was between 0.2 and 0.7 during the

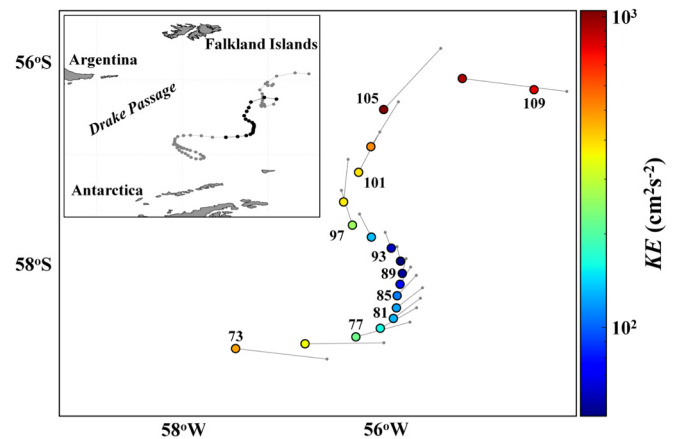


Fig. 4. Biofloat locations during the observational period (DOY 73–109) colored by the OSCAR derived kinetic energy per unit mass (KE) at each location. For each biofloat location, the likely surface trajectory over the course of two days (grey line and dots) was derived from the daily OSCAR currents. The DOY is labelled next to every other biofloat location. The inset shows the biofloat trajectory over the entire deployment period with the observational period in black which corresponds with the biofloat trajectory in the larger figure.

observational period (Supplemental Fig. 3), which suggests that the quasi-lagrangian approach to this dataset is likely reasonable.

Acoustic Doppler Current Profiler transects across the Drake Passage (Renault et al., 2011) show that the currents in the upper 1000 m are on the order of 50 cm s^{-1} and decrease to order 10 cm s^{-1} below 1000 m. We therefore assume that while the biofloat was at or below the park depth of 1000 m ($\sim 34 \text{ h}$ within a profiling cycle) the ambient currents were approximately 10 cm s^{-1} and while the biofloat was above the park depth it experienced ambient currents of 50 cm s^{-1} . Based on these assumptions, we estimate that a hypothetical float would have travelled $\sim 38 \text{ km}$ during one profiling cycle, whereas a hypothetical parcel of water in the surface ocean would have travelled $\sim 86 \text{ km}$. The ratio between the hypothetical float and surface parcel motion is 0.44, which falls within the range of observed D_{if} to D_i ratios, and indicates that the biofloat trajectory may have lagged the OSCAR surface currents by a factor of 2.

3. Results and discussion

3.1. Quasi-lagrangian observations of a naturally occurring phytoplankton bloom

Biofloat [Chl] and [POC] observations show a marked increase just after the profile on DOY 73, indicating the presence of a naturally occurring phytoplankton bloom (Fig. 3). The observed bloom is followed by organic carbon export (deep spikes in [Chl] and [POC] in Fig. 3; more on this topic in Section 3.2) lasting through the profile on DOY 109.

Fig. 5 shows the time series of depth integrated [Chl] and [POC] above the MLD, denoted $[Chl]_{MLD}$ and $[POC]_{MLD}$, respectively. On DOY 73, the $[POC]_{MLD}$ was $1.4 \times 10^3 \text{ mg m}^{-2}$, which is within one standard deviation of the mean $[POC]_{MLD}$ ($2.1 \times 10^3 \pm 1.0 \times 10^3$) measured during the biofloat deployment period. Between DOY 73 and the peak $[POC]_{MLD}$ on DOY 89, the observed $[POC]_{MLD}$ increased to $6.5 \times 10^3 \text{ mg m}^{-2}$ while the $[Chl]_{MLD}$ also increased from 7.3 mg m^{-2} to 43.7 mg m^{-2} . The maximum $[Chl]_{MLD}$ and $[POC]_{MLD}$ both occurred on DOY 89, herein referred to as the peak bloom.

Satellite derived surface chlorophyll-*a* observations leading up to and during the observational period were sparse for both MODIS and VIIRS sensors. Fig. 6 shows the available three-day composite MODIS-Aqua Chlorophyll Concentration's (NASA, 2018) between DOY 65 and DOY 105. For this analysis, daily 4 km, Level 3 MODIS-Aqua Chlorophyll Concentrations (OCI Algorithm) were averaged into three day

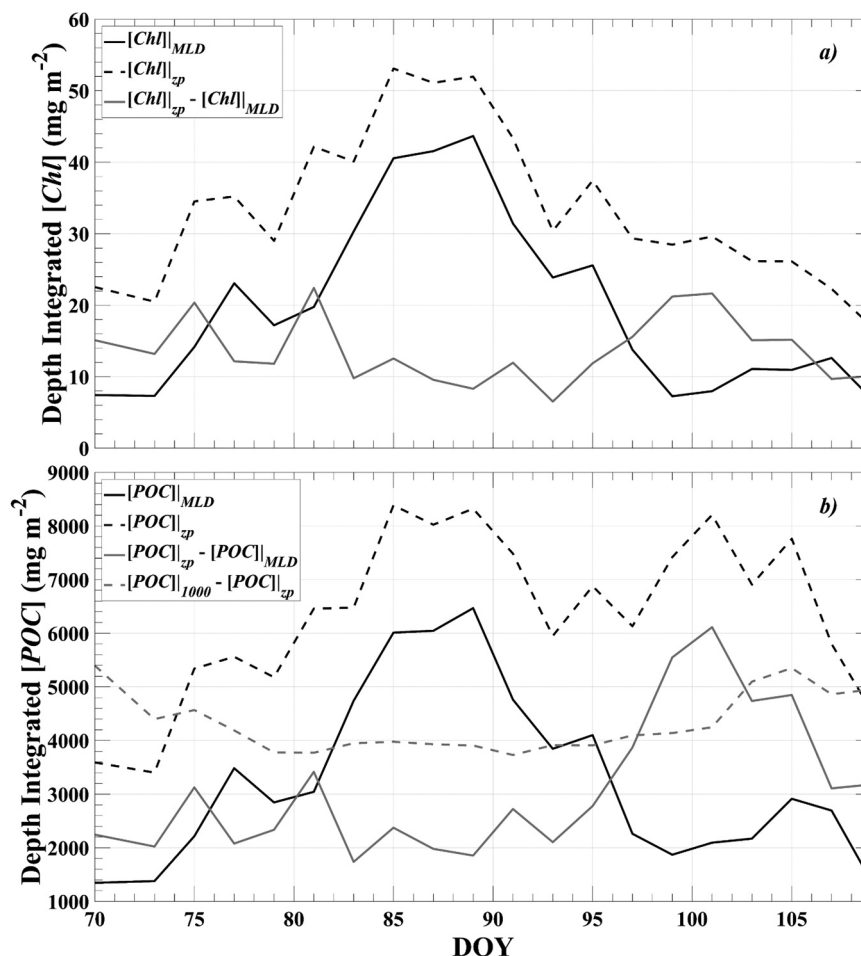


Fig. 5. The time series of the depth integrated a) chlorophyll concentration, $[Chl]$, and b) particulate organic carbon concentration, $[POC]$, above the mixed layer depth (MLD; solid black line), above the depth of the reference isopycnal (z_p ; dashed black line), between the MLD and z_p (solid grey line; $[Chl]_{z_p} - [Chl]_{MLD}$ or $[POC]_{z_p} - [POC]_{MLD}$), and between 1000 m and z_p (dashed grey line; $[POC]_{1000} - [POC]_{z_p}$ only).

composites to increase spatial coverage (e.g. the product on DOY 79 encompasses data between DOY 78 and DOY 80; we are choosing to display MODIS-Aqua because it had slightly better coverage than VIIRS). The MODIS-Aqua surface chlorophyll observations on DOY 79 confirm the existence of the phytoplankton bloom observed by the biofloat on DOY 79. On that date, the satellite derived surface chlorophyll concentration at the biofloat location was $\sim 0.3 \text{ mg m}^{-3}$ which compares favorably with the MLD averaged biofloat chlorophyll concentration, $\langle [Chl] \rangle_{MLD}$, of 0.44 mg m^{-3} . However, the lack of satellite observations prior to DOY 79 makes it difficult to judge if the float drifted into an existing phytoplankton bloom, if an existing bloom overtook the biofloat trajectory, or if a phytoplankton bloom developed within the waters being transported along the quasi-Lagrangian biofloat trajectory.

The challenge in interpreting and analyzing patterns in the observed bloom and export is the lack of contextual observations (both in-situ and satellite derived) that might provide clues as to whether to treat this data as primarily a time series or a spatial series. This problem, however, is not exclusive to this study. Under the assumed quasi-Lagrangian framework, there are two possible analysis approaches: (1) To consider the biofloat dataset as a time series whereby the high frequency profiling mission allowed the biofloat to closely track mesoscale ocean process, and therefore observe the development of the phytoplankton bloom, and (2) To consider the dataset spatially whereby the biofloat trajectory moved into or was overtaken by an existing phytoplankton bloom. We proceed in the following subsections by exploring these analysis approaches.

3.1.1. Analyzing the biofloat bloom observations with respect to time

The mechanisms controlling surface ocean phytoplankton abundance in the SO include seasonal light availability, episodic micro-nutrient supply, rapid changes in the mixed layer or critical depth, and grazing. We do not observe evidence of rapid shallowing of the mixed layer depth prior to bloom formation (Figs. 2 and 3) and seasonal light availability was decreasing throughout the observational period (Supplemental Fig. 2a), suggesting that the bloom was not a result of alleviating seasonal light limitation. The SO is a HNLC region where surface iron concentrations have been shown to be a limiting factor for phytoplankton blooms (Martin, 1990; Martin et al., 1990; Venables and Moore, 2010), including in the Drake Passage (Hoffmann et al., 2006). The observed surface iron concentrations in the Drake Passage generally range from 0.1 to $0.2 \text{ nmol Fe l}^{-1}$ (Martin et al., 1990; Klunder et al., 2014).

We estimate that the net growth rate of $[Chl]_{MLD}$, r , between subsequent profiles ($\Delta t = t_1 - t_0$) following Behrenfeld (2010). The mean r between DOY 73 and 89 was 0.11 day^{-1} , which is similar to previously observed rates in the SO (Boyd et al., 2000; Abbott et al., 2001). Note that within the net growth rate estimate are other unaccounted for processes (e.g. grazing, remineralization, advection and spatial changes, etc.), and therefore the specific growth rate was likely different.

$$r = \frac{\ln([Chl]_{MLD1}) - \ln([Chl]_{MLD0})}{\Delta t} \quad (2)$$

The estimated bloom growth rate (Eq. (2)) compares favorably with

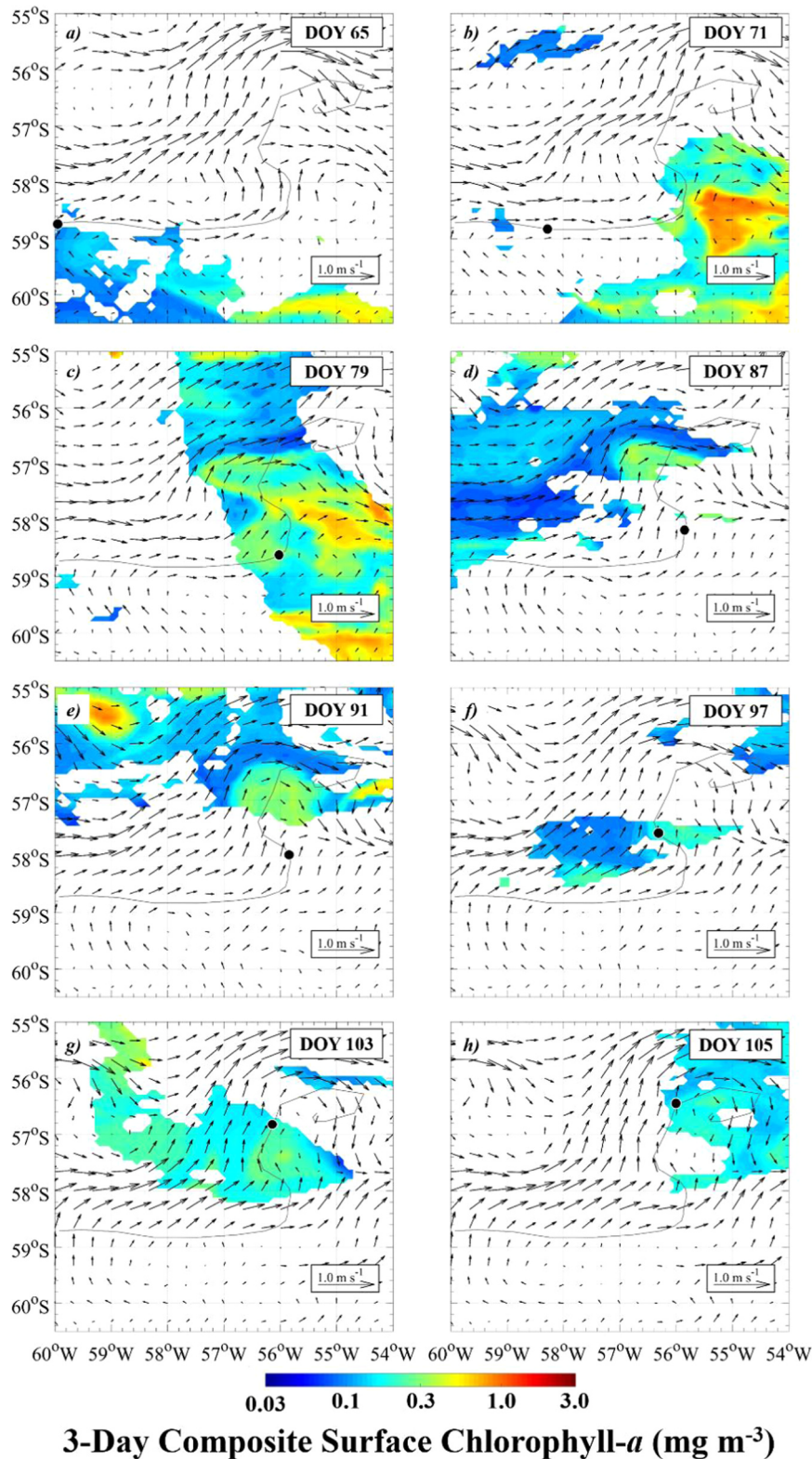


Fig. 6. Three-day composite MODIS-Aqua chlorophyll concentrations (NASA, 2018) on select days leading up to and during the observational period. The biofloat trajectory between DOY 63 and 113 is plotted (thin line) along with the biofloat location on that DOY (black dots).

the biological response following artificial surface ocean iron fertilization. The Southern Ocean iron-release experiment (SOIREE) observed a six fold increase in the depth integrated chlorophyll-*a* within ten days of initial (and continued) iron injection (Boyd et al., 2000). During the Southern Ocean Iron Experiment (SOFeX), profiling biofloats observed a fourfold increase in particulate organic carbon (Bishop et al., 2004)

over similar timescales. We therefore proceed in this subsection exploring natural sources of dissolved iron that may have influenced the biofloat trajectory and fueled bloom development. These include northward advection of iron-rich water from the Antarctic shelf, upwelling from beneath the ferricline, exchanges in the vicinity of fronts, and wet-iron deposition from the atmosphere.

Interactions between currents and topographic features in the HNLC SO enhance biological production via the direct terrestrial injection of dissolved iron (Blain et al., 2001; Venables et al., 2007) and upwelling of iron from below the ferricline (e.g. Nolting et al., 1991; Comiso et al., 1993; Holm-Hansen et al., 2005) which is between 300 and 500 m in the Drake Passage (Martin et al., 1990; Klunder et al., 2014; Tagliabue et al., 2014) and is deeper than the MLDs during the observational period (Fig. 2). Sokolov and Rintoul (2007) showed that the western edge of chlorophyll-*a* blooms within the Antarctic Circumpolar Current (ACC) in the Drake Passage are associated with topographically forced upwelling regions, with blooms persisting along streamlines downstream. However, in the days leading-up to the peak bloom (DOY 75–89), the biofloat did not encounter any significant bathymetric features (Fig. 1) and we therefore have no evidence to support an injection of iron into the surface ocean from terrestrial sources or from below the ferricline.

Klunder et al. (2014) suggested that patchy areas of increased dissolved iron in the Drake Passage region may be the result of new iron deposition from precipitation events with air mass origins over the South American continent. Indeed, ice core (Basile et al., 1997; McConnell et al., 2007), atmospheric modelling (Li et al., 2008), and remote sensing (Boyd et al., 2012) studies suggest that the Patagonia region of South America is a significant source of iron to the Drake Passage region via atmospheric deposition.

Between DOY 78 and 86 atmospheric reanalysis products (Kalnay et al., 1996) show that the mean 925 mb wind over the Drake Passage spanned $10.0\text{--}15.0\text{ m s}^{-1}$ and off the South American continent, while the mean precipitation rates were $5.0\text{--}6.0\text{ mm day}^{-1}$ (Fig. 7b). In contrast, the previous period from DOY 71–78 (Fig. 7a) featured zonal winds across the Drake Passage and no rainfall over the biofloat locations. In addition, the HYbrid Single-Particle Lagrangian Integrated Trajectory (HYSPLIT; Stein et al., 2015) three day backward trajectories

show that the air at 1500 m ($\approx 850\text{ mb}$) and 3000 m ($\approx 700\text{ mb}$) above the biofloat locations originated from the South American continent in the days preceding DOY 79 and 81. However, the lag time between the potential iron deposition and peak bloom in this study was only five to seven days, and half of what Bishop et al. (2002) observed during an aerial deposition event in the HNLC North Pacific. Furthermore, the NASA TOMS Aerosol Index does not indicate a strong aerosol signal that would be indicative of an iron deposition event (Supplemental Fig. 2b). Assuming 0.045 m of rainfall between DOY 78 and 86, we estimate an upper 50 m freshening approximately $0.03\text{--}0.04\text{ psu}$ (all else being equal) whereas a freshening of nearly twice that amount was observed (Fig. 2c). While this could also indicate higher rainfall totals than portrayed by the model, evidence for wet iron deposition is inconclusive.

As the southern branch of the ACC approaches Shackleton Transverse Ridge (STR), flow is diverted southward and through the Shackleton Gap (SG; see Fig. 1 for geographic reference). As the flow exits the SG, it splits into a coherent northward-flowing jet along the east side of the STR and a meandering band of mesoscale eddies that propagate north-eastward and toward the main ACC stream (Zhou et al., 2010). The latter of these features is capable of advecting the iron-rich water (Hopkinson et al., 2007) from the Antarctica shelf into the Ona Basin and southern Drake Passage which can enhance phytoplankton productivity (Zhou et al., 2010; Frants et al., 2013a; Ardyna et al., 2017). However, the mean currents derived from drifter data (Zhou et al., 2010) suggest that the north-eastward transport of the surface Antarctic coastal water becomes incoherent north of 60°S , and therefore it is unclear whether this mechanism is capable of consistently advecting iron as far north as the observed bloom in this study. Indeed the mean OSCAR currents between DOY 75 and 89 also lack a defined advective signature north 60°S (Fig. 8). Therefore, we have no conclusive evidence that horizontal advection of dissolved iron from the Antarctic shelf intersected the biofloat trajectory in the days leading up to the observed bloom.

The TS diagram (Fig. 9) shows a coherent winter water mass signature between 100 and 200 m which matches previous observations of the waters just south of the Polar Front (PF), and within the Antarctic Zone (Gordon et al., 1977). Both the TS diagram (Fig. 9) and sea surface temperatures (Fig. 8) show that the biofloat was south of the Polar Front (PF) leading up to and during the observational period. However, phytoplankton blooms (Moore and Abbott, 2000, 2002) and higher dissolved iron concentrations are often observed in the vicinity fronts in the SO and may be attributed to a variety of processes including advection and stretching, cross-frontal mixing (Lutjeharms et al., 1985; Dufour et al., 2015) and meander- or eddy-induced upwelling (Abbott et al., 2001; Marshall and Speer, 2012). It is therefore possible that unresolved cross-frontal, filament, or eddy mixing processes could have supplied the dissolved iron in the days leading up to the bloom,

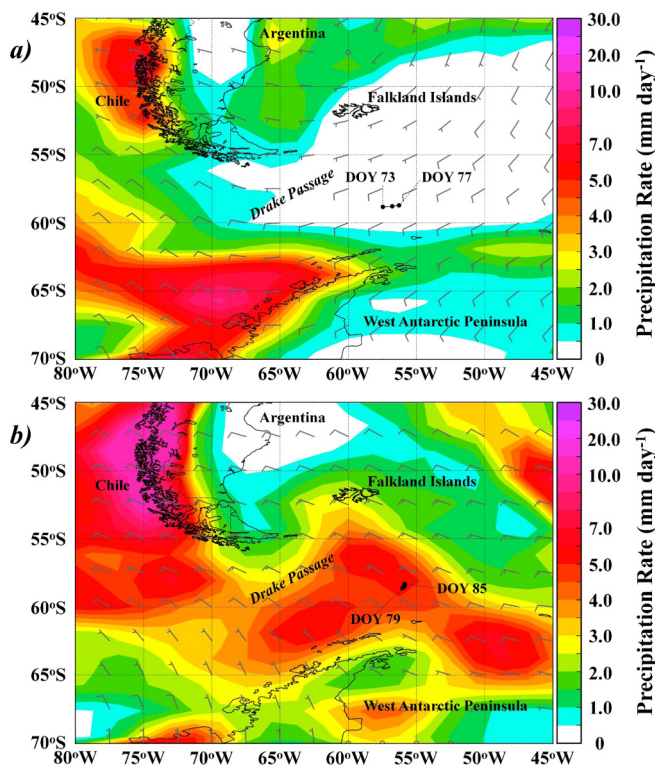


Fig. 7. Mean surface precipitation rate (contoured) and 935 mb winds (barbs) for a) DOY 71–78 and b) DOY 78–86 from the NOAA National Center for Environmental Prediction Reanalysis (Kalnay et al., 1996). Corresponding float locations are plotted.

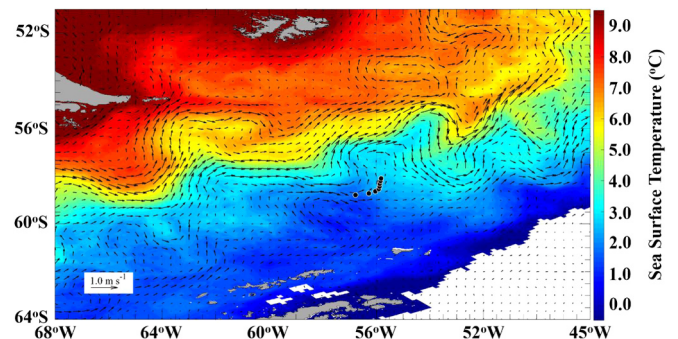


Fig. 8. Averaged daily Level-4 multi-scale ultra-high resolution (MUR) sea surface temperature (SST) observations (colored; JPL MUR MEASURE (2010)) and OSCAR currents (quivers) between DOY 75 and 89. The corresponding biofloat locations are plotted.

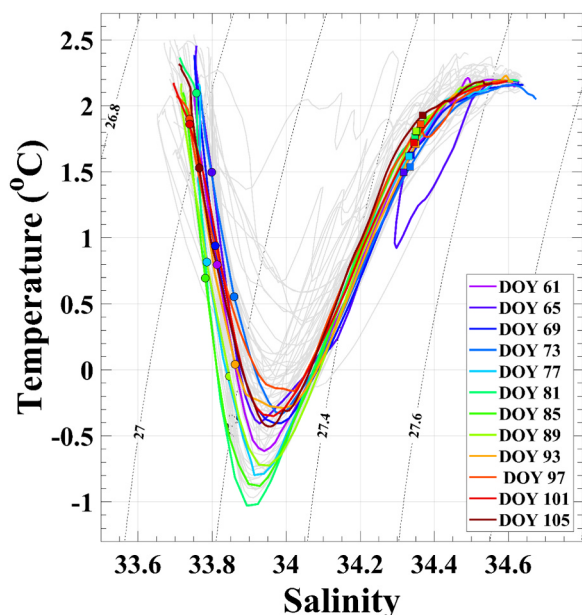


Fig. 9. Temperature-salinity biofloat profiles in the upper 500 m throughout the deployment period (light grey) are plotted in σ_t (kg m^{-3}) space (dashed black contours) with select biofloat profiles leading up to and during the observational period colored. The MLD (circles) and z_p (squares) for each select biofloat profile are also plotted.

however the TS profiles (Fig. 9) spanning DOY 65–75 do not support mixing of water masses.

3.1.2. Analyzing the biofloat bloom observations with respect to space

The assumption that profiling floats are quasi-Lagrangian with respect to surface mesoscale processes (Llort et al., 2018), and that the SO is an equivalent barotropic system (Killworth and Hughes, 2002; Gille et al., 2007), also implies that floats do not exactly track the speed or direction of surface currents. This was evident in our study because the ratio of D_f to D_l was not consistent (Supplemental Fig. 3). The largest ratios during the observational period occurred in the days leading up to the peak bloom (DOY 75–85) and, as shown in Fig. 4, the directional

difference between the biofloat trajectory and the surface tracers during that period was the greatest. This implies that the biofloat trajectory during this period likely deviated from the surface ocean currents. Or, alternatively, that the OSCAR currents, with a native resolution of five days, were unable to resolve all relevant oceanic processes.

In the days leading up to the observational period (beginning on DOY 73), the MODIS-Aqua surface chlorophyll data was limited along the biofloat trajectory (Fig. 6a, b). However, there was a bloom located at approximately 55.25°W and 58.5°S on DOY 71. The highest chlorophyll concentrations associated with this feature were just east of the would-be biofloat locations between DOY 81 and 89, which was coincident with the highest biofloat [Chl] and [POC] surface ocean observations (Fig. 5).

The clearly defined bloom east of the biofloat trajectory on DOY 71 still existed on DOY 79, however the magnitude and defined spatial coherence of the feature had decreased (Fig. 6c). Empirically it appears that part of this bloom (and/or the dissolved iron supply) was advected into, and around, a cyclonic eddy to the northwest of the feature. Indeed, the high chlorophyll signal remained within the cyclonic eddy as it drifted east between DOY 79 and 91 (Fig. 6c-e). The sharp gradient in chlorophyll concentration north of the eddy was coincident with the strongest currents and SST gradient (Fig. 8), and likely indicated the location of the PF.

The TS diagram (Fig. 9) shows that while the biofloat remained south of the PF, it likely did not stay within the exact same water mass throughout the observational period; the winter water signature on DOY 77 through 89 (coincident with the timing of the bloom) was colder than the days prior and after by approximately 0.5 °C (Figs. 2a and 9). This subtle change in thermohaline properties decreased the spiciness within the temperature minimum layer (Fig. 2d), suggesting the float may have drifted into a different water mass. The cooler temperature minimum layer is indicative of a water mass with origins near the Antarctic shelf. Shelf water is high in dissolved iron concentration (Hopkinson et al., 2007; Measures et al., 2013) and has been observed in and beyond the Ona Basin (Frants et al., 2013b). The location of the Southern ACC Front (SAACF) often serves as the barrier between the high and low nutrient waters (Frants et al., 2013b).

In the absence of a conclusive theory for bloom development in Section 3.1.1, we speculate that the quasi-Lagrangian biofloat may have drifted into an existing bloom south of the PF or, alternatively, that the

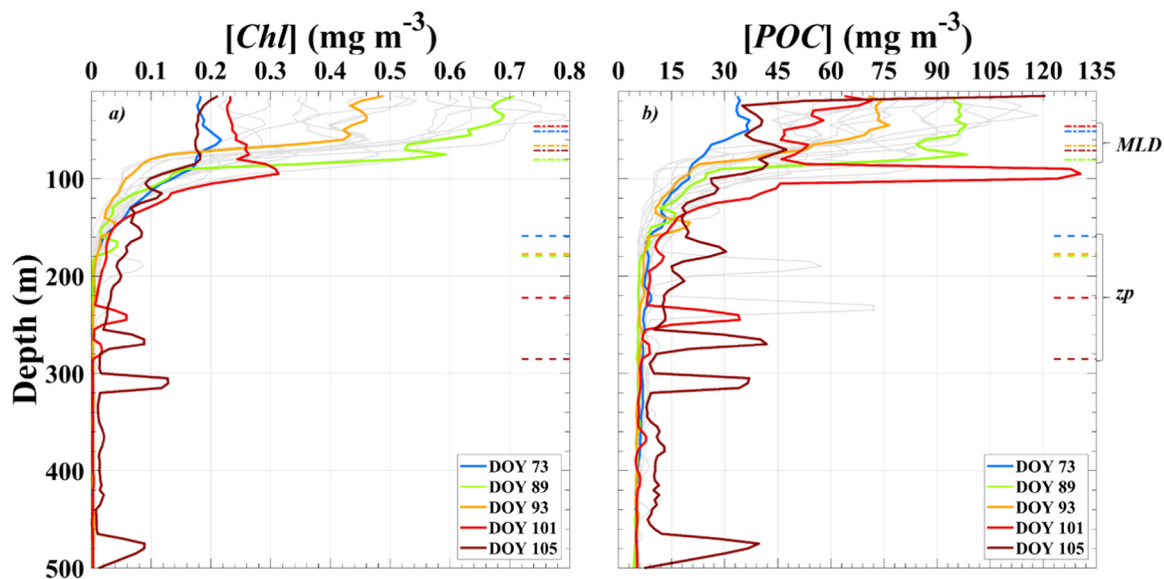


Fig. 10. a) Chlorophyll concentration ([Chl]) and b) particulate organic carbon concentration ([POC]) profiles on select days during the observational period to show the naturally occurring phytoplankton bloom and organic carbon export. The horizontal marks on the right, vertical axis show the MLD (dash-dot line) and z_p (dash line) corresponding to each profile (coordinating colors).

biofloat may have been overtaken by an existing bloom from the west as suggested in Fig. (6c). These competing horizontal advective theories are supported by subtle changes in the thermohaline properties. The TS diagram further suggests that the observed water mass during the bloom may have originated along the iron-rich Antarctic shelf.

3.2. Bloom termination and export

In the days following the peak bloom (DOY 89–93), there was a significant loss in depth integrated $[POC]$ and $[Chl]$ above the MLD, which was followed by enhanced carbon export through DOY 109 (Fig. 3; denoted by deep $[POC]$ and $[Chl]$ spikes). During the export period (herein defined between DOY 89 and 109) the ratio of D_{if} to D_t was low (generally below 0.5), the biofloat directionally tracked the surface currents (Fig. 4 and Supplemental Movie), and spiciness in the surface ocean was consistent profile-to-profile (Fig. 2d). This indicates that the equivalent barotropic assumption is reasonable profile-to-profile during the export period (i.e. the biofloat may have slightly lagged the surface), and at a minimum, the quasi-Lagrangian biofloat likely resolved mesoscale processes, including the eddy the float was in (Figs. 4 and 6).

Supplementary material related to this article can be found online at doi:10.1016/j.dsr.2019.02.004.

Vertical $[POC]$ and $[Chl]$ profiles in Fig. 10 indicate that the decrease in surface ocean phytoplankton abundance is approximately uniform with depth between DOY 89 and 93. Indeed both $[Chl]_{MLD}$ and $[POC]_{MLD}$ decreased at similar rates during this period (45% and 41%, respectively) while the depth integrated $[POC]$ and $[Chl]$ above z_p , $[Chl]_{z_p}$ and $[POC]_{z_p}$, also decreased by 42% and 28%, respectively. We interpret this to indicate that the loss in surface ocean $[Chl]$ over this span was not due to changes in intracellular pigment concentrations. Furthermore, Figs. (3) and (5) show that the loss was likely not due to direct organic carbon export between DOY 89 and 93. One interpretation is that the loss in surface phytoplankton abundance may be the result of grazing, although the biofloat may also have been influenced by other water masses (Figs. 2 and 9).

Between DOY 93 and 105, the biofloat was pulled into, and closely tracked, a cyclonic eddy just south of the PF (Figs. 4, 6, and the Supplemental movie). As a result, the KE increased from $62 \text{ cm}^2 \text{ s}^{-2}$ to $1045 \text{ cm}^2 \text{ s}^{-2}$ and z_p deepened from 175 to 289 m with near uniform change in profile-to-profile isopycnal spacing below the MLD (Fig. 2c). The difference between the depth integrated $[POC]$ and $[Chl]$ above the MLD and z_p between DOY 93 and 105 (Fig. 5) indicates that the phytoplankton abundance originally above the MLD accumulated between the two layers. The $[Chl]$ and $[POC]$ profiles on DOY 101 show a localized sub-surface maximum with lower phytoplankton abundance shallower in the water column (Fig. 10). The export of large, sinking aggregates of organic matter and phytoplankton into the deep ocean occurred between DOY 103 and 109 as biofloat circumnavigated the eddy (Fig. 6), the KE increased (Fig. 4), and z_p further deepened (Fig. 2). Coincident deep $[Chl]$ and $[POC]$ spikes on DOY 105 (Fig. 10) are indicative of aggregated phytoplankton (Briggs et al., 2011) that rapidly sink out of the surface ocean (Turner, 2002; Smetacek et al., 2012). The MODIS-Aqua surface chlorophyll observations were sparse during this period (Fig. 6), however they indicate a decrease in surface chlorophyll over time within the eddy which supports the biofloat observed loss of surface ocean phytoplankton abundance.

Eddies can also enhance the export of small particles through subduction. For example, Omand et al. (2015) presented evidence for post-bloom subduction of small, non-sinking POC particulates along sloping isopycnal surfaces on the perimeter of mesoscale eddies. The resulting vertical velocities of these aggregates were on the order of 30 m day^{-1} and can account of up to 25% of the total carbon export through remineralization. Omand et al. (2015) isolated non-sinking particulates from larger, sinking aggregates of organic matter by vertically smoothing spikes in the backscatter signal. In this study we opted to

retain higher frequency signal (Section 2.1), but nevertheless observed (Figs. 2, 3, 5 and 10) subsurface deepening of the upper ocean $[Chl]$ and $[POC]$ signal that was coincident with the uniform deepening of isopycnals (Grenier et al., 2015) as the biofloat profiled along the edge of the mesoscale eddy.

In addition to remineralization of smaller phytoplankton, eddy-driven subduction and the deepening of isopycnals was likely important in the export of aggregates. POC biomass is distributed among cells of all sizes (Richardson and Jackson, 2007) which infers that large phytoplankton aggregates were likely also subducted as their neutral density points deepened—which alone may have aided in export by deepening the starting point for gravitational settling of phytoplankton and aggregates. It is important to note that for large aggregates, the contribution from this processes is likely less than that of direct sinking whereby particle sinking rates are on the order of 100 m day^{-1} (Fischer and Karakas, 2009; Bishop and Wood, 2009; Briggs et al., 2011). Eddy-driven subduction likely aided export by deepening the neutral density points of aggregates, potentially decoupling the phytoplankton aggregates from grazing pressure, and reducing light availability.

The carbon export observations in this study parallel some aspects of the high frequency biofloat observations in Bishop and Wood (2009; herein BW09), specifically when comparing Fig. 10 in this study to Fig. 10 in BW09. BW09 observed deep POC concentrations coincident with deeper isohalines and isotherms (BW09 Figs. 4 and 7) indicating that subduction and changes in particle neutral density points may be important. However, BW09 did not find evidence of strong direct carbon export, potentially due to a lack of supporting observation in the preceding days.

3.2.1. Export estimate

During the peak bloom on DOY 89 the $[POC]_{z_p}$ was $8.3 \times 10^3 \text{ mg m}^{-2}$ with 77%, or $6.4 \times 10^3 \text{ mg m}^{-2}$, of that above the MLD (Fig. 5b). By DOY 109, just after the export event, $[POC]_{z_p}$ fell by $3.7 \times 10^3 \text{ mg m}^{-2}$, representing a 44.5% net loss of $[POC]$ above z_p . We observe the highest depth integrated $[POC]$ between z_p and 1000 m on DOY 105 (Fig. 5b), which is coincident with the export signal (Figs. 3 and 10). Between DOY 89 and 105 we observed an increase of depth integrated $[POC]$ between z_p and 1000 m of $1.5 \pm 0.3 \times 10^3 \text{ mg m}^{-2}$. We interpret this estimate as a lower bound for direct POC export out of the surface ocean. Applying the $\pm 20\%$ error in POC estimations from Johnson et al. (2017b), this represents $\sim 40 \pm 22\%$ of the net loss of POC above z_p between DOY 89 and 109, and $\sim 18 \pm 10\%$ of the total $[POC]_{z_p}$ observed during the peak bloom. However, based on the experimental design of this study (specifically the quasi-Lagrangian nature of the biofloat), it is impossible to know what fraction of the observed export is a temporary effect of the eddy.

An enhancement in the depth integrated $[POC]$ between z_p and 1000 m is not observed until \sim DOY 100 (Fig. 3b). If we assume direct export began on this day and lasted through DOY 105, we estimate an export rate of $\sim 250 \pm 50 \text{ mg m}^{-2} \text{ d}^{-1}$ from above z_p . Our estimate is on the same order of magnitude of observed export rates, which are between 50 and $400 \text{ mg m}^{-2} \text{ d}^{-1}$ (e.g. Buesseler and Boyd, 2009; Briggs et al., 2011). The observed export below z_p appears to be a combination of direct export and export due to subduction along the edge of a mesoscale eddy. While our estimate of net surface ocean export ($\sim 18 \pm 10\%$) is based on a single event, it is remarkably similar to export estimates using the gradient of particulate organic nitrogen and nitrate from SOCCOM floats across the SO ($\sim 19\%$; Stukel and Ducklow, 2017). It is also similar to the upper bound estimate of eddy subduction driven export in the SO ($\sim 19\%$) based on observations of apparent oxygen utilization, spiciness, and particulate organic carbon (Llort et al., 2018).

4. Summary and concluding remarks

In summary, an APEX biofloat profiling every two days within the

high mesoscale kinetic energy Drake Passage observed a naturally occurring phytoplankton bloom and carbon export event in 2013 between DOY 73 and 109, which is at the end of the austral growing season. Throughout our analysis we assumed that the biofloat is quasi-Lagrangian with respect to the surface ocean mesoscale circulation (Llort et al., 2018). We therefore pursued temporal and spatial analysis approaches of the biofloat dataset, recognizing we could not simultaneously control for changes in both. Treating the dataset as a time series, we investigated potential sources of new iron that could have intersected the quasi-Lagrangian biofloat trajectory and fueled the observed bloom. Our analysis rejected dissolved iron injection into the surface ocean from below the ferricline. However, the evidence was inconclusive regarding wet iron deposition, advection of iron from the Antarctic shelf, or unresolved sub-mesoscale mixing processes in the vicinity of the PF. Treating the dataset as a spatial series, MODIS-Aqua surface chlorophyll observations and the TS diagram suggest that the quasi-Lagrangian biofloat may have drifted into an existing phytoplankton bloom or, alternatively, that a phytoplankton bloom drifted over the biofloat. We adopted the theory that horizontal advective processes relative to the biofloat trajectory were the most probable explanation for the observed bloom, but this lacks the supporting the observations required for a definitive conclusion.

Following the bloom, our results suggest that eddy-driven subduction and a change in the vertical structure of the upper ocean water column were important in the time period leading up to carbon export. Export was observed between DOY 103 and 109 with deep spikes in $[POC]_{lp}$ that indicate export of large aggregates from the surface ocean (Briggs et al., 2011). We estimate that $\sim 40 \pm 22\%$ of the observed loss in $[POC]_{lp}$ was likely the result of direct carbon export. Furthermore, we estimate that $\sim 18 \pm 10\%$ of the peak bloom $[POC]$ on DOY 89 was exported through DOY 105 in part, related to effects of eddy subduction. This event-scale export estimate is remarkably similar to composite, basin-scale export estimates across the SO (Stukel and Ducklow, 2017; Llort et al., 2018), suggesting the community is closer to resolving the eddy-driven carbon export component of the SO carbon cycle.

The quasi-Lagrangian nature of this, and other like autonomous float studies, offer only generalizations based on the available in-situ, remotely sensed, and model data; due to its nature, this study likely suffers from a lack of replication. BW09 noted that relatively low-cost, ensemble biofloat deployments at the same location would likely yield more meaningful information about the relationship between the biogeochemical processes, physical forcing mechanisms (e.g. surface processes, hydrography, fronts, etc.) and the biological pump. Grenier et al. (2015) provides a good example of this analysis approach and employed profiling floats with shallower park depths that were therefore more likely to track surface processes. Similarly, high frequency profiling biofloats provide meaningful vertical information, that when coupled with high resolution (temporally and spatially) satellite data, could offer new insights into the biological response to mesoscale processes, including the effect of eddy-driven subduction on carbon export in highly energetic SO environments.

Acknowledgements

This research was funded through the University of Delaware, College of Earth, Ocean, and Environment's Charles and Patricia Robertson Research Fund. We thank Jim McClintock for assistance in float deployment. MUR SST data were provided by JPL under support by NASA MEaSUREs program and freely accessible at: <https://mur.jpl.nasa.gov/>. PAR and MODIS-Aqua data were provided by The NASA Ocean Biological Processing Group (OBGP) and freely accessible at: <https://oceancolor.gsfc.nasa.gov>. OMI/Aura Aerosol Index data were provided through the NASA Earth Science Data and Information System (ESDIS) project and freely accessible at: https://disc.sci.gsfc.nasa.gov/datasets/OMTO3d_V003/summary?keywords=Aerosol%20Index. OMI/Aura Aerosol Index data were provided through the NASA Earth

Science Data and Information System (ESDIS) project with support from Earth and Space Research (ESR) and freely accessible at: https://podaac.jpl.nasa.gov/dataset/OSCAR_L4_OC_third-deg. NCEP Reanalysis data were provided by the NOAA/OAR/ESRL PSD and freely accessible at <http://www.esrl.noaa.gov/psd/>. The authors gratefully acknowledge the NOAA Air Resources Laboratory (ARL) for use of the HYSPLIT transport and dispersion model and READY website (<http://www.ready.noaa.gov>) used in this publication. The biofloat data is available upon request: moliver@udel.edu or adavies@usna.edu. A.R.D. would like to thank Pablo Huq, Robert Vaillancourt, A. Denny Kirwan, Joseph P. Smith, Megan Cimino, Danielle Haulsee, Matthew Breece, Patricia Ryan, and paper reviewers for constructive discussions; your input undoubtedly improved this manuscript.

Appendix A. Supporting information

Supplementary data associated with this article can be found in the online version at [doi:10.1016/j.dsr.2019.02.004](https://doi.org/10.1016/j.dsr.2019.02.004).

References

- Abbott, M.R., Richman, J.G., Bartlett, J.S., Barksdale, B.S., 2001. Meanders in the Antarctic Polar Frontal Zone and their impact on phytoplankton. *Deep Sea Res. Part II: Top. Stud. Oceanogr.* 48, 3891–3912.
- Ardyna, M., Claustre, H., Sallee, J.-B., D'Ovidio, F., Gentili, B., van Dijken, G., D'Ortenzio, F., Arrigo, K.R., 2017. Delineating environmental control of phytoplankton biomass and phenology in the Southern Ocean. *Geophys. Res. Lett.* 44, 5016–5024. <https://doi.org/10.1002/2016GL072428>.
- Argo Science Team, (1998), On the design and Implementation of Argo - an initial plan for the 639 global array of profiling floats. International CLIVAR Project Office Report, 21, 32.
- Arrigo, K.R., van Dijken, G.L., Bushinsky, S., 2008. Primary production in the Southern Ocean, 1997–2006. *J. Geophys. Res.-Oceans* 113 (C8). <https://doi.org/10.1029/2007JC004551>.
- Basile, I., Grousset, F.E., Revel, M., Petit, J.R., Biscaye, P.E., Barkov, N.I., 1997. Patagonian origin of glacial dust deposited in East Antarctica during glacial stages 2, 4 and 6. *Earth Planet. Sci. Lett.* 146, 573–589.
- Behrenfeld, M., 2010. Abandoning Sverdrup's Critical Depth Hypothesis on phytoplankton blooms. *Ecology* 91, 977–989.
- Bishop, J.K., Wood, T.J., 2009. Year-round observations of carbon biomass and flux variability in the Southern Ocean. *Glob. Biogeochem. Cycles* 23. <https://doi.org/10.1029/2008GB003206>.
- Bishop, J.K.B., Wood, T.J., 2008. Particulate matter chemistry and dynamics in the twilight zone at VERTIGO ALOHA and K2 sites. *Deep-Sea Res.* 55, 1684–1706. <https://doi.org/10.1016/j.dsr.2008.07.012>.
- Bishop, J.K.B., Davis, R.E., Sherman, J.T., 2002. Robotic observations of dust storm enhancement of carbon biomass in the North Pacific. *Science* 298 (5594), 817–821. <https://doi.org/10.1126/science.1074961>.
- Bishop, J.K.B., Wood, T.J., Davis, R.E., Sherman, J.T., 2004. Robotic observations of enhanced carbon biomass and export at 55 degrees S during SOFeX. *Science* 304 (5669), 417–420. <https://doi.org/10.1126/science.1087717>.
- Blain, S., Treguer, P., Belviso, S., 2001. A biogeochemical study of the island mass effect in the context of the iron hypothesis: Kerguelen Islands, Southern Ocean. *Deep-Sea Res.* 48, 163–187.
- Blain, S., Quéguiner, B., Armand, L., Belviso, S., Bombled, B., Bopp, L., Bowie, A., Brunet, C., Brussaard, C., Carlotti, F., Christaki, U., Corbière, A., Durand, I., Ebersbach, F., Fuda, J., Garcia, N., Gerringa, L., Griffiths, B., Guigue, C., Guiller, C., Jaquet, S., Jeandel, C., Laan, P., Lefèvre, D., Lo Monaco, C., Malits, A., Mosseri, J., Obernosterer, I., Park, Y., Picheral, M., Pondaven, P., Remenyi, T., Sandroni, V., Sarthou, G., Savoye, N., Scouarnec, L., Souhaut, M., Thuiller, D., Timmermans, K., Trull, T., Uitz, J., van Beek, P., Veldhuis, M., Vincent, D., Viollier, E., Vong, L., Wagener, T., 2007. Effect of natural iron fertilization on carbon sequestration in the Southern Ocean. *Nature* 446, 1070–1074. <https://doi.org/10.1038/nature05700>.
- Bonjean, F., Lagerloef, G.S.E., 2002. Diagnostic model and analysis of the surface currents in the tropical Pacific Ocean. *J. Phys. Oceanogr.* 32, 2938–2954.
- Boss, E., Guidi, L., Richardson, M.J., Stemmann, L., Gardner, W., Bishop, J.K.B., Anderson, R.F., Sherrell, R.M., 2015. Optical techniques for remote and in-situ characterization of particles pertinent to GEOTRACS. *Prog. Oceanogr.* 133, 43–45. <https://doi.org/10.1016/j.pocean.2014.09.007>.
- Boyd, P.W., Watson, A.J., Law, C.S., Abraham, E.R., Trull, T., Murdoch, R., Bakker, D.C.E., Bowie, A.R., Buesseler, K.O., Chang, H., Charette, M., Croot, P., Downing, K., Frew, R., Gall, M., Hadfield, M., Hall, J., Harvey, M., Jameson, G., LaRoche, J., Liddicoat, M., Ling, R., Maldonado, M.T., McKay, R.M., Nodder, S., Pickmere, S., Pridmore, R., Rintoul, S., Safi, K., Sutton, P., Strzepek, R., Tanneberger, K., Turner, S., Waite, A., Zeldis, J., 2000. A mesoscale phytoplankton bloom in the polar Southern Ocean stimulated by iron fertilization. *Nature* 407, 695–702. <https://doi.org/10.1038/35037500>.
- Boyd, P.W., Arrigo, K.R., Strzepek, R., Dijken, G.L., 2012. Mapping phytoplankton iron utilization: insights into Southern Ocean supply mechanisms. *J. Geophys. Res.* 117,

- C06009. <https://doi.org/10.1029/2011JC007726>.
- Briggs, E., Martz, T.R., Talley, L.D., Mazloff, M.R., Johnson, K.S., 2017. Physical and biological drivers of biogeochemical tracers within the seasonal sea ice zone of the Southern Ocean from profiling floats. *J. Geophys. Res. Oceans* 123. <https://doi.org/10.1002/2017JC012846>.
- Briggs, N., Perry, M.J., Cetini, C.I., Lee, C., D'Asaro, E., Gray, A.M., Rehm, E., 2011. High-resolution observations of aggregate flux during a sub-polar North Atlantic spring bloom. *Deep Sea Res. Part I: Oceanogr. Res. Pap.* 58 (10), 1031–1039. <https://doi.org/10.1016/j.dsr.2011.07.007>.
- Buesseler, K.O., Boyd, P.W., 2009. Shedding light on processes that control particle export and flux attenuation in the twilight zone of the open ocean. *Limnol. Oceanogr.* 54 (4), 1210–1232.
- Coale, K.H., Johnson, K.S., Chavez, F.P., Buesseler, K.O., Barber, R.T., Brzezinski, M.A., Cochlan, W.P., Millero, F.J., Falkowski, P.G., Bauer, J.E., Wanninkhof, R.H., Kudela, R.M., Altabet, M.A., Hales, B.E., Takahashi, T., Landry, M.R., Bidigare, R.R., Wang, X., Chase, Z., Strutton, P.G., Friederich, G.E., Gorbunov, M.Y., Lance, V.P., Hiltling, A.K., Hiscock, M.R., Demarest, M., Hiscock, W.T., Sullivan, K.F., Tanner, S.J., Gordon, R.M., Hunter, C.N., Elrod, V.A., Fitzwater, S.E., Jones, J.L., Tozzi, S., Koblizek, M., Roberts, A.E., Herndon, J., Brewster, J., Ladizinsky, N., Smith, G., Cooper, D., Timothy, D., Brown, S.L., Selph, K.E., Sheridan, C.C., Twining, B.S., Johnson, Z.I., 2004. Southern Ocean iron enrichment experiment: carbon cycling in high- and low-Si waters. *Science* 304 (5669), 408–414. <https://doi.org/10.1126/science.1089778>.
- Comiso, J.C., McClain, C.R., Sullivan, C.W., Ryan, J.P., Leonard, C.L., 1993. 388 Coastal zone color scanner pigment concentrations in the Southern Ocean and relationships to geophysical surface features. *J. Geophys. Res.-Oceans* 98 (C2), 2419–2451. <https://doi.org/10.1029/92JC02505>.
- Daniault, N., Menard, Y., 1985. Eddy kinetic energy distribution in the Southern Ocean from altimetry and FGGE drifting buoys. *J. Geophys. Res.-Oceans* 90 (C6), 11877–11889. <https://doi.org/10.1029/JC090iC06p11877>.
- Dong, S., Sprintall, J., Gille, S.T., Talley, L., 2008. Southern Ocean mixer-layer depth from Argo float profiles. *J. Geophys. Res.-Oceans* 113, C06013. <https://doi.org/10.1029/2006JC004051>.
- Dufour, C.O., Griffies, S.M., de Souza, G.R., Frenger, I., Morrison, A.K., Palter, J.B., Sarmiento, J.L., Galbraith, E.D., Dunne, J.P., Anderson, W.G., Slater, R.D., 2015. Role of mesoscale eddies in cross-frontal transport of heat and biogeochemical tracers in the Southern Ocean. *J. Phys. Oceanogr.* 45, 3057–3081.
- El-Sayed, S., 1987. Productivity of the Antarctic Waters—a reappraisal. In: Holm-Hansen, O., Bolis, L., Gilles, R. (Eds.), *Marine Phytoplankton and Productivity*. Springer-Verlag, Berlin, Germany, pp. 19–34. <https://doi.org/10.1029/LN008p0019>.
- ESR, 2009. OSCAR third degree resolution ocean surface currently. Ver. 1. PO.DAAC, CA, USA. <http://dx.doi.org/10.5067/OSCAR-03D01>.
- Fischer, G., Karakas, G., 2009. Sinking rates and ballast composition of particles in the Atlantic Ocean: implications for the organic carbon fluxes to the deep ocean. *Biogeosciences* 6 (1), 85–102. <https://doi.org/10.5194/bg-6-85-2009>.
- Flament, P., 2002. A state variable for characterizing water masses and their diffusive stability: spiciness. *Prog. Oceanogr.* 54, 493–501.
- Frants, M., Gille, S.T., Hatta, M., Hiscock, W.T., Kahru, M., Measures, C.I., Mitchell, B.G., Zhou, M., 2013a. Analysis of horizontal and vertical processes contributing to natural iron supply in the mixed layer in the southern Drake passage. *Deep-Sea Res. Part II* 90, 68–76.
- Frants, M., Gille, S.T., Hewes, C.D., Holm-Hansen, O., Kahru, M., Lombrozo, A., Measures, C.I., Mitchell, B.G., Wang, H., Zhou, M., 2013b. Optimal multiparameterization analysis of source water distribution in the Southern Drake Passage. *Deep-Sea Res. Part II* 90, 31–42.
- Gervais, F., Riebesell, U., Gorbunov, M.Y., 2002. Changes in primary productivity and chlorophyll-a in response to iron fertilization in the Southern Polar Frontal Zone. *Limnol. Oceanogr.* 47 (5), 1324–1335. <https://doi.org/10.4319/lo.2002.47.5.1324>.
- Gill, A.E., 1982. Appendix Three - Properties of Seawater, in *Atmosphere-Ocean Dynamics*. International Geophysics Series Academic Press, pp. 599–603. [https://doi.org/10.1016/S0074-6142\(08\)60041-8](https://doi.org/10.1016/S0074-6142(08)60041-8).
- Gille, S.T., Speer, K., Ledwell, J.R., Naveira Garabato, A.C., 2007. Mixing and stirring in the Southern Ocean. *Eos Trans. AGU* 88, 382–383. <https://doi.org/10.1029/2007EO390002>.
- Gordon, A.L., Georgi, D.T., Taylor, H.W., 1977. Antarctic polar frontal zone in the Western Scotia Sea – summer 1975. *J. Phys. Oceanogr.* 7, 309–328.
- Grenier, M., Della Penna, A., Trull, T.W., 2015. Autonomous profiling float observations of the high-biomass plume downstream of the Kerguelen Plateau in the Southern Ocean. *Biogeosciences*. <https://doi.org/10.5194/bg-12-27072015>.
- Haëntjens, N., Boss, E., Talley, L.D., 2017. Revisiting Ocean Color algorithms for chlorophyll a and particulate organic carbon in the Southern Ocean using biogeochemical floats. *J. Geophys. Res.-Oceans* 122 (8), 6583–6593.
- Harvey, M.J., Law, C.S., Smith, M.J., Hall, J.A., Abraham, E.R., Stevens, C.L., Hadfield, M.G., Ho, D.T., Ward, B., Archer, S.D., Caine, J.M., Currie, K.I., Devries, D., Ellwood, M.J., Hill, P., Jones, G.B., Katz, D., Kuparinen, J., Macaskill, B., Main, W., Marriner, A., McGregor, J., McNeil, C., Minnett, P.J., Nodder, S.D., Pelouquin, J., Pickmere, S., Pinkerton, M.H., Safi, K.A., Thompson, R., Walkington, M., Wright, S.W., Ziolkowski, L.A., 2010. The SOLAS air–sea gas exchange experiment (SAGE). *Deep-Sea Res. Part II* 753–763.
- Hennon, T.D., Riser, S.C., Mecking, S., 2016. Profiling float-based observations of net respiration beneath the mixed layer. *Glob. Biogeochem. Cycles* 30, 920–932. <https://doi.org/10.1002/2016GB005380>.
- Hiscock, W.T., Millero, F.J., 2005. Nutrient and carbon parameters during the Southern Ocean iron experiment (SOFEX). *Deep-Sea Res. Pt. I* 52, 2086–2108.
- Hoffmann, L.J., Peeken, I., Lochte, K., Assmy, P., Veldhuis, M., 2006. Different reactions to Southern Ocean phytoplankton size classes to iron fertilization. *Limnol. Oceanogr.* 51 (3), 1217–1229. <https://doi.org/10.4319/lo.2006.51.3.1217>.
- Holm-Hansen, O., Kahru, M., Hewes, C.D., 2005. Deep chlorophyll a maxima (DCMs) in pelagic Antarctic waters. ii. relation to bathymetric features and dissolved iron concentrations. *Mar. Ecol. Prog. Ser.* 297, 71–81. <https://doi.org/10.3354/meps297071>.
- Hopkinson, B.M., Mitchell, B.G., Reynolds, R.A., Wang, H., Sleph, K.E., Measures, C.I., Hewes, C.D., Holm-Hansen, O., Barbeau, K.A., 2007. Iron limitation across chlorophyll gradients in the southern Drake passage: phytoplankton response to iron addition and photosynthetic indicators or iron stress. *Limnol. Oceanogr.* 52 (6), 2540–2554.
- Johnson, K.S., Plant, J.N., Coletti, L.J., Jannasch, H.W., Sakamoto, C.M., Riser, S.C., Swift, D.D., Williams, N.L., Boss, E., Haëntjens, N., Talley, L.D., Sarmiento, J.L., 2017b. Biogeochemical sensor performance in the SOCCOM profiling float array. *J. Geophys. Res.-Oceans* 122 (8), 6416–6436.
- Johnson, K.S.J.N., Plant, L.D., Talley, J.L., Sarmiento, 2017. Annual nitrate drawdown observed by SOCCOM profiling floats and the relationship to annual net community productivity. *J. Geophys. Res.-Oceans*. <https://doi.org/10.1002/2017JC012839>.
- Jones, J.M., Gille, S.T., Goosse, H., Abram, N.J., Canziani, P.O., Charman, D.J., Clem, K.R., Crosta, X., de Lavergne, C., Eisenman, I., England, M.H., Fogt, R.L., Frankcombe, L.M., Marshall, G.J., Masson-Delmotte, V., Morrison, A.K., Orsi, A.J., Raphael, M.N., Renwick, J.A., Schneider, D.P., Simpkins, G.R., Steig, E.J., Stenni, B., Swingedouw, D., Vance, T.R., 2016. Assessing recent trends in high-latitude Southern Hemisphere surface climate. *Nat. Clim. Change* 6, 917–926. <https://doi.org/10.1038/NCLIMATE3103>.
- JPL MUR MEASURES Project, 2010. GHRSSST Level 4 MUR Global Foundation Sea Surface Temperature Analysis. PO.DAAC, CA, USA. Dataset accessed [20 June 2017] at https://mur.jpl.nasa.gov/images_global.php.
- Kalnay, E., Kanamitsu, M., Kistler, R., Collins, W., Deaven, D., Gandin, L., Iredell, M., Saha, S., White, G., Woollen, J., Zhu, Y., Leetmaa, A., Reynolds, R., Chelliah, M., Ebisuzaki, W., Higgins, W., Janowiak, J., Mo, K.C., Ropelewski, C., Wang, J., Jenne, R., Joseph, D., 1996. The NCEP/NCAR 40-year reanalysis project. *Bull. Am. Meteorol. Soc.* 77, 437–471.
- Kamenkovich, I., Haza, A., Gray, A.R., Dufour, C.O., Garraffo, Z., 2017. Importance of mesoscale eddies and mean circulation in ventilation of the Southern Ocean. *J. Geophys. Res. Oceans* 122. <https://doi.org/10.1002/2017JC012819>.
- Killworth, P.D., Hughes, C.W., 2002. The Antarctic Circumpolar Current as a free equivalent-barotropic jet. *J. Mar. Res.* 60, 19–45.
- Klunder, M.B., Laan, P., Baar, H.J.W.D., Middag, R., Neven, I., Ooijen, J.V., 2014. Dissolved Fe across the Weddell Sea and Drake Passage: impact of DFe on nutrient uptake. *Biogeosciences* 11 (3), 651–669. <https://doi.org/10.5194/bg-11-651-2014>.
- Law, C.S., Smith, M.J., Stevens, C.L., Abraham, E.R., Ellwood, M.J., Hill, P., Nodder, S., Pelouquin, J., Pickmere, S., Safi, K., Walkington, C.M., 2011. Did dilution limit the phytoplankton response to iron addition in HNLC/Si sub-Antarctic waters during the SAGE experiment? *Deep-Sea Res. Pt. II* 58, 786–799.
- Li, F., Ginoux, P., Ramaswamy, V., 2008. Distribution, transport, and deposition of mineral dust in the Southern Ocean and Antarctica: contribution of major sources. *J. Geophys. Res.-Atmos.* 113 (D10). <https://doi.org/10.1029/2007JD009190>.
- Llort, J., Langlais, C., Matear, R., Moreau, S., Lenton, A., Strutton, P.G., 2018. Evaluating Southern Ocean carbon eddy-pump from biogeochemical-argo floats. *J. Geophys. Res.-Oceans* 123, 971–984. <https://doi.org/10.1002/2017JC012861>.
- Lutjeharms, J.R.E., Walters, N.M., Allanson, B.R., 1985. Oceanic frontal systems and biological enhancement in Antarctic Nutrient Cycles and Food Webs, edited by Siegfried, W.R., et al. Springer-Verlag, New York, 1985.
- Marshall, J., Speer, K., 2012. Closure of the meridional overturning circulation through Southern Ocean upwelling. *Nat. Geosci.* 5 (3), 171–180. <https://doi.org/10.1038/neg1391>.
- Martin, J.H., 1990. Glacial-interglacial CO₂ change: the iron hypothesis. *Paleoceanography* 5 (1), 1–13. <https://doi.org/10.1029/PA005i001p00001.433>.
- Martin, J.H., Gordon, R.M., Fitzwater, S.E., 1990. Iron in Antarctic waters. *Nature* 345, 156–159. <https://doi.org/10.1038/345156a0>.
- Martin, P., van der Loeff, M.R., Cassar, N., Vandromme, P., d'Ovidio, F., Stemann, L., Rengarajan, R., Soares, M., González, H.E., Ebersbach, F., Lampitt, R.S., Sanders, R., Barnett, B.A., Smetacek, V., Naqvi, S.W.A., 2013. Iron fertilization enhanced net community production but not downward particle flux during the Southern Ocean iron fertilization experiment LOHAFEX. *Glob. Biogeochem. Cycles* 27, 871–881.
- Mazloff, M.R., Sallée J.-B., Menezes V.V., Macdonald, A.M., Meredith, M.P., Newman, L., Pellichero, V., Roquet, F., Swart, S., Wählin, A., 2017. Southern Ocean [in State of the Climate 2016]. *Bull. Am. Meteorol. Soc.*
- McConnell, J.R., Aristarain, A.J., Banta, J.R., Edwards, P.R., Simoes, J.C., 2007. 20th-Century doubling in dust archived in an Antarctica Peninsula ice core parallels climate change and desertification in South America. *Proc. Natl. Acad. Sci. USA* 104 (5742).
- Measures, C.I., Brown, M.T., Sleph, K.E., Apprill, A., Zhou, M., Hatta, M., Hiscock, W.T., 2013. The influences of shelf processes in delivering dissolved iron to the HNLC waters of the Drake Passage, Antarctica. *Deep-Sea Res. Part II* 90, 77–88. <https://doi.org/10.1016/j.dsr.2.2012.11.994>.
- Moore, J.K., Abbott, M.R., 2000. Phytoplankton chlorophyll distributions and primary production in the Southern Ocean. *J. Geophys. Res.-Oceans* 105 (C12), 28709–28722. <https://doi.org/10.1029/1999JC000004>.
- Moore, J.K., Abbott, M.R., 2002. Surface chlorophyll concentrations in relation to the Antarctic Polar Front: seasonal and spatial patterns from satellite observations. *J. Mar. Syst.* 37 (13), 69–86. [https://doi.org/10.1016/S0924-7963\(02\)00196-3](https://doi.org/10.1016/S0924-7963(02)00196-3).
- NASA, 2018. Goddard Space Flight Center, Ocean Ecology Laboratory, Ocean Biology Processing Group. Moderate-resolution Imaging Spectroradiometer (MODIS) Aqua Chlorophyll Data; 2018 Reprocessing, NASA OB.DAAC, Greenbelt, MD, USA. <https://doi.org/10.5067/AQUA/MODIS/L3B/CHL/2018>. (Accessed on 20 June

- 2017).
- Nolting, R.F., Baar, H.J.W.D., Bennekou, A.J.V., Masson, A., 1991. Cadmium, copper and iron in the Scotia Sea, Weddell Sea and Weddell/Scotia Confluence (Antarctica). *Mar. Chem.* 35 (14), 219–243. [https://doi.org/10.1016/S0304-4203\(09\)90019-6](https://doi.org/10.1016/S0304-4203(09)90019-6).
- Ollitraul, M., Rannou, J., 2013. ANDRO: an Argo-based deep displacement dataset. *J. Atmos. Oceanic Technol.* 759–788. <https://doi.org/10.1175/JTECH-D-12-00073.1>.
- Omand, M.M., D'Asaro, E.A., Lee, C.M., Perry, M.J., Briggs, N., Cetinic, I., Mahadevan, A., 2015. Eddy-driven subduction exports particulate organic carbon from the spring bloom. *Science* 348 (6231), 222–225. <https://doi.org/10.1126/science.1260062>.
- Pollard, R.T., Salter, I., Sanders, R.J., Lucas, M.L., Moore, M.C., Mills, R.A., Statham, P.J., Allen, J.T., Baker, A.R., Bakker, D.C.E., Charette, M.A., Fielding, S., Fones, G.R., French, M., Hickman, A.E., Holland, R.J., Hughes, J.A., Jickells, T.D., Lampitt, R.S., Morris, P.J., Nédélec, F.H., Nielsdóttir, M., Planquette, H., Popova, E.E., Poulton, A.J., Read, J.F., Seeyave, S., Smith, T., Stinchcombe, M., Taylor, S., Thomalla, S., Venables, H.J., Williamson, R., Zubkov, M.V., 2009. Southern Ocean deep-water carbon export enhanced by natural iron fertilization. *Nature* 457, 577–580. <https://doi.org/10.1038/nature07716>.
- Rembauville, M., Briggs, N., Ardyna, M., Uitz, J., Catala, P., Penkerch, C., Poteau, A., Claustre, H., Blain, S., 2017. Plankton assemblage estimated with BGC-Argo floats in the Southern Ocean: implications for seasonal successions and particle export. *J. Geophys. Res.: Oceans* 122 (10), 8278–8292.
- Renault, A., Provost, C., Sennéchal, N., Barré, N., Kartavtseff, A., 2011. Two full-depth velocity sections in the Drake Passage in 2006—Transport estimates. *Deep Sea Res. Part II* 58, 2572–2591. <https://doi.org/10.1016/j.dsr2.2011.01.004>.
- Richardson, T.L., Jackson, G.A., 2007. Small phytoplankton and carbon export from the southern ocean. *Science* 315 (58113), 838–840.
- Riser, S.C., Freeland, H.J., Roemmich, D., Wijffels, S., Troisi, A., Belbéoch, M., Gilbert, D., Xu, J., Pouliquen, S., Thresher, A., Traon, P.L., Maze, G., Klein, B., Ravichandran, M., Grant, F., Poulan, P., Suga, T., Lim, B., Sterl, A., Sutton, P., Mork, K., Vélez-Belchí, P.J., Ansong, I., King, B., Turton, J., Baringer, M., Jayne, S.R., 2016. Fifteen years of ocean observations with the global Argo array. *Nat. Clim. Change* 6, 145–153. <https://doi.org/10.1038/nclimate2872>.
- Roesler, C., Uitz, J., Claustre, H., Boss, E., Xing, X., Organelli, E., Briggs, N., Bricaud, A., Schmechtig, C., Poteau, A., D'Ortenzio, F., Ras, J., Drapeau, S., Haentjens, N., Barbieux, M., 2017. Recommendations for obtaining unbiased chlorophyll estimates from in situ chlorophyll fluorometers: a global analysis of WET Labs ECO. *Sens. Limnol. Oceanogr. Methods* 15, 572–585. <https://doi.org/10.1002/lom3.10185>.
- Smetacek, V., Klaas, C., Strass, V.H., Assmy, P., Montresor, M., Cisewski, B., Savoye, N., Webb, A., d'Ovidio, F., Arrieta, J.M., Bathmann, U., Bellerby, R., Berg, G.M., Croot, P., Gonzalez, S., Henjes, J., Herndl, G.J., Hoffmann, L.J., Leach, H., Losch, M., Mills, M.M., Neill, C., Peeken, I., Rottgers, R., Sachs, O., Sauter, E., Schmidt, M.M., Schwarz, J., Terbruggen, A., Wolf-Gladrow, D., 2012. Deep carbon export from a Southern Ocean iron-fertilized diatom bloom. *Nature* 487, 313–319. <https://doi.org/10.1038/nature11229>.
- Sokolov, S., Rintoul, S.R., 2007. On the relationship between fronts of the Antarctic Circumpolar Current and surface chlorophyll concentrations in the Southern Ocean. *J. Geophys. Res.-Oceans* 112 (C7). <https://doi.org/10.1029/2006JC004072>.
- Stein, A.F., Draxler, R.R., Rolph, G.D., Stunder, B.J.B., Cohen, M.D., Ngan, F., 2015. NOAA's HYSPLIT atmospheric transport and dispersion modeling system. *Bull. Am. Meteorol. Soc.* 96, 2059–2077. <https://doi.org/10.1175/BAMS-D-14-00110.1>.
- Stukel, M.R., Ducklow, H.W., 2017. Stirring up the biological pump: vertical mixing and carbon export in the Southern Ocean. *Glob. Biogeochem. Cycles* 31, 1420–1431. <https://doi.org/10.1002/2017GB005652>.
- Tagliabue, A., Sallee, J., Bowie, A.R., Levy, M., Swart, S., Boyd, P.W., 2014. Surface-water iron supplies in the Southern Ocean sustained by deep winter mixing. *Nat. Geosci.* 7, 314–320. <https://doi.org/10.1038/ngeo2101>.
- Turner, J.T., 2002. Zooplankton fecal pellets, marine snow and sinking phytoplankton blooms. *Aquat. Microb. Ecol.* 27, 57–102. <https://doi.org/10.3354/ame027057>.
- Venables, H., Moore, C.M., 2010. Phytoplankton and light limitation in the Southern Ocean: learning from high-nutrient, high-chlorophyll areas. *J. Geophys. Res.-Oceans* 115 (C2). <https://doi.org/10.1029/2009JC005361>.
- Venables, H.J., Pollard, R.T., Popova, E.E., 2007. Physical conditions controlling the development of a regular phytoplankton bloom north of the Crozet Plateau, Southern Ocean. *Deep-Sea Res.: Part II* 54, 1949–1965.
- Wessel, P., Smith, W.H.F., 1996. A global, self-consistent, hierarchical, high-resolution shoreline database. *J. Geophys. Res.* 101, 8741–8743.
- Williams, N.L., Juranek, L.W., Feely, R.A., Johnson, K.S., Sarmiento, J.L., Talley, L.D., Russell, J.L., Riser, S.C., Dickson, A.G., Gray, A.R., Wanninkhof, R., Takeshita, Y., 2017. Calculating surface ocean pCO₂ from biogeochemical Argo floats equipped with pH: an uncertainty analysis. *Glob. Biogeochem. Cycles* 31 (3). <https://doi.org/10.1002/2016GB005541>.
- Williams, N.L., Juranek, L.W., Feely, R.A., Russell, J.L., Johnson, K.S., Hales, B., 2018. Assessment of the carbonate chemistry seasonal cycles in the Southern Ocean from persistent observational platforms. *J. Geophys. Res. Oceans*. <https://doi.org/10.1029/2017JC012917>.
- Zhou, M., Zhu, Y., Dorland, R.D., Measures, C.I., 2010. Dynamics of the current system in the southern Drake Passage. *Deep Sea Res. Part I: Oceanogr. Res. Pap.* 57 (9), 1039–1048. <https://doi.org/10.1016/j.dsr.2010.05.012>.